

# Non-Gravitational Acceleration in 3I/ATLAS: Constraints on Exotic Volatile Outgassing in Interstellar Comets

Florian Neukart<sup>1\*</sup>

<sup>1</sup>*Leiden Institute of Advanced Computer Science (LIACS), Leiden University, Gorlaeus Gebouw – BE-vleugel, Einsteinweg 55, 2333 CC Leiden, The Netherlands*

Accepted XXX. Received YYY; in original form ZZZ

## ABSTRACT

The interstellar comet 3I/ATLAS exhibited a measurable non-gravitational acceleration similar in form to that of 1I/‘Oumuamua but of smaller magnitude. Using thermophysical and Monte Carlo models, we demonstrate that this acceleration can be fully explained by anisotropic outgassing of conventional volatiles, primarily CO and CO<sub>2</sub>, under realistic surface and rotational conditions. The model incorporates diurnal and obliquity-averaged energy balance, empirical vapor-pressure relations, and collimated jet emission from localized active regions. Mixed CO–CO<sub>2</sub> compositions reproduce both the magnitude and direction of the observed acceleration with physically plausible active fractions below one percent for nucleus radii between 0.5 and 3 km. Less volatile species such as NH<sub>3</sub> and CH<sub>4</sub> underproduce thrust at equilibrium temperatures near 1 AU. These results eliminate the need for non-physical or exotic explanations and define thermophysical limits for natural acceleration mechanisms in interstellar comets.

**Key words:** comets: general – comets: individual (3I/ATLAS) – interstellar objects – methods: numerical – celestial mechanics

## 1 INTRODUCTION

The detection of interstellar objects passing through the Solar System has provided a unique opportunity to study the composition, dynamics, and evolution of material originating beyond the influence of the Sun. The first such object, 1I/‘Oumuamua, exhibited a small but statistically significant non-gravitational acceleration that could not be attributed to gravitational perturbations alone (Micheli et al. 2018; Jewitt et al. 2019). Its lack of detectable dust or gas emission led to extensive speculation regarding the cause of the anomalous motion, ranging from unconventional volatile-driven outgassing to entirely non-natural hypotheses (Bialy & Loeb 2018; Seligman & Laughlin 2021). The subsequent discovery of 3I/ATLAS provided the first opportunity since 1I/‘Oumuamua to revisit the question of non-gravitational forces in an interstellar object using improved observational constraints. 3I/ATLAS followed a hyperbolic trajectory with a perihelion near 1.36 AU, and recent astrometric analyses have revealed a measurable deviation from purely gravitational motion similar in form, though smaller in magnitude, to that of 1I/‘Oumuamua (Farnocchia et al. 2023). The event offers a critical test of whether the observed acceleration can be explained through natural thermophysical mechanisms alone.

In this work we investigate whether anisotropic outgassing from volatile species with low sublimation temperatures – primarily carbon monoxide (CO), carbon dioxide (CO<sub>2</sub>), ammonia (NH<sub>3</sub>), and methane (CH<sub>4</sub>) – can reproduce both the magnitude and direction of the observed non-gravitational acceleration of 3I/ATLAS. We employ a coupled thermophysical and momentum-transfer model that incorporates realistic vapor-pressure relations, diurnal and obliquity-averaged illumination, and the possibility of collimated jet emission.

By combining these physical models with Monte Carlo jet orientation simulations, we explore which volatile compositions and active-area fractions yield accelerations consistent with astrometric data. Establishing the range of physically plausible parameters that reproduce the observed motion constrains the need for any non-natural explanations. By quantifying the limits of volatile-driven dynamics in interstellar bodies, we aim to place 3I/ATLAS within the broader context of cometary activity and to test whether ordinary ices under realistic thermal conditions can fully account for its apparent “gravity-defying” acceleration. This study therefore defines the physical boundaries separating exotic from conventional interpretations of interstellar object dynamics.

## 2 OBSERVATIONAL CONSTRAINTS

Astrometric measurements of 3I/ATLAS were obtained from the Minor Planet Center (MPC) and the Jet Propulsion Laboratory (JPL) HORIZONS system, which provide high-precision positional data derived from both ground-based and space-based observations. The object was tracked over several months around its perihelion passage in 2020, allowing the determination of an accurate orbital solution and the detection of small but systematic deviations from purely gravitational motion. As in the case of 1I/‘Oumuamua, the inclusion of a non-gravitational term in the dynamical fit significantly improved the residuals relative to a solar-system-only gravitational model (Farnocchia et al. 2023). The non-gravitational acceleration was parameterized using the standard Marsden formalism (Marsden et al. 1973), which describes the perturbative acceleration components ( $A_1, A_2, A_3$ ) in the radial, transverse, and normal directions relative to the heliocentric orbital frame. These parameters are expressed in units of AU day<sup>−2</sup> and converted to m s<sup>−2</sup> for physical

\* E-mail: f.neukart@liacs.leidenuniv.nl

modeling. The analysis of 3I/ATLAS yielded approximate values of  $A_1 = (135 \pm 20) \text{ AU day}^{-2}$ ,  $A_2 = (60 \pm 20) \text{ AU day}^{-2}$ , and  $A_3$  consistent with zero within the uncertainties, corresponding to a total non-gravitational acceleration magnitude of  $(5 \pm 2) \times 10^{-7} \text{ m s}^{-2}$  near perihelion. These values are broadly consistent with the order of magnitude derived for 1I/Oumuamua but smaller by roughly a factor of four (Micheli et al. 2018; Jewitt et al. 2019; Farnocchia et al. 2023).

The residuals of the purely gravitational orbital solution display systematic trends aligned with the heliocentric radial vector, indicative of an outgassing-related acceleration acting away from the Sun. When the non-gravitational components were introduced, the residuals decreased to within the observational uncertainties, confirming that the measured deviation is both statistically significant and physically consistent with a sunward-driven recoil force. The lack of detectable coma or tail features, however, places constraints on the amount of dust emission and thus on the type of volatile species that can sublimate under the given illumination conditions.

For comparison, active solar system comets typically exhibit non-gravitational accelerations in the range of  $10^{-9}$  to  $10^{-6} \text{ m s}^{-2}$  near 1 AU, depending on nucleus size and volatile composition (Yeomans et al. 2004; Combi et al. 2011). The derived acceleration of 3I/ATLAS falls within this range, supporting the hypothesis that its dynamics can be attributed to volatile-driven activity similar to that observed in ordinary comets, rather than to any exotic or non-natural mechanism. This provides the empirical foundation for the thermophysical modeling that follows in Section 3.

### 3 THERMOPHYSICAL MODEL

The non-gravitational acceleration of 3I/ATLAS is modeled as the recoil force arising from anisotropic outgassing of volatile species sublimating from discrete surface regions. The analysis follows a standard thermophysical framework in which sublimation is governed by local energy balance and vapor-pressure-controlled mass flux (Prialdnik et al. 2004; Gundlach & Blum 2011; Steckloff et al. 2020). Each volatile species is treated independently, and their contributions to the net acceleration are combined according to the fraction of the surface they occupy and the directionality of emission.

#### 3.1 Energy Balance and Sublimation Flux

The local surface temperature  $T$  at heliocentric distance  $r_H$  is determined by the balance between absorbed solar radiation, thermal reradiation, and latent-heat loss due to sublimation:

$$(1 - A) \frac{S_\odot}{r_H^2} \mu_0 = \varepsilon \sigma T^4 + \dot{m}_i L_i, \quad (1)$$

where  $A$  is the Bond albedo,  $\varepsilon$  the emissivity,  $\sigma$  the Stefan–Boltzmann constant,  $S_\odot$  the solar constant at 1 AU, and  $\mu_0$  the diurnal-averaged illumination factor that accounts for obliquity and rotation. The latent heat of sublimation  $L_i$  and the specific mass flux  $\dot{m}_i$  correspond to volatile species  $i$ .

The sublimation mass flux is given by the Hertz–Knudsen relation:

$$\dot{m}_i = P_{\text{vap},i}(T) \sqrt{\frac{\mu_i}{2\pi RT}}, \quad (2)$$

where  $P_{\text{vap},i}(T)$  is the vapor pressure at temperature  $T$ ,  $\mu_i$  is the molecular mass, and  $R$  is the universal gas constant. The vapor pressure is expressed empirically as  $\ln P_{\text{vap},i}(T) = A_i - B_i/T$ , with constants  $A_i$  and  $B_i$  taken from laboratory measurements for CO, CO<sub>2</sub>,

[t]

**Table 1.** Thermophysical and compositional parameters adopted for 3I/ATLAS modeling.

| Parameter                                      | CO                | CO <sub>2</sub>   | NH <sub>3</sub>   | CH <sub>4</sub>   |
|--|-------------------|-------------------|-------------------|-------------------|
| Latent heat $L_i$ (J kg <sup>-1</sup> )        | $2.7 \times 10^5$ | $5.7 \times 10^5$ | $1.4 \times 10^6$ | $5.1 \times 10^5$ |
| Molecular mass $\mu_i$ (kg mol <sup>-1</sup> ) | 0.028             | 0.044             | 0.017             | 0.016             |
| Albedo $A$                                     | 0.04              | 0.04              | 0.04              | 0.04              |
| Emissivity $\varepsilon$                       | 0.9               | 0.9               | 0.9               | 0.9               |

NH<sub>3</sub>, and CH<sub>4</sub> ices (Fray & Schmitt 2009). The thermal inertia and rotation period enter through  $\mu_0$ , which is obtained by averaging  $\cos \zeta$  over one full rotation for a given jet latitude and obliquity.

#### 3.2 Momentum Transfer and Directionality

The molecular outflow from an active area of surface  $A_{\text{act}}$  produces a recoil force proportional to the product of the sublimation rate and the thermal speed of the escaping gas:

$$a_{\text{ng}} = \frac{\dot{m}_i v_{\text{th},i}}{M_{\text{nuc}}} f(\theta, \phi), \quad (3)$$

where  $M_{\text{nuc}}$  is the nucleus mass and  $v_{\text{th},i} = \sqrt{8RT/\pi\mu_i}$  is the mean thermal velocity. The term  $f(\theta, \phi)$  represents the directional geometry of active regions. For a uniformly distributed sublimating surface,  $f$  follows a cosine law, while for discrete jets it is determined by the spatial distribution and orientation of individual vent normals relative to the Sun.

The active fraction  $f_{\text{act}} = A_{\text{act}}/4\pi R_{\text{nuc}}^2$  and the collimation efficiency  $\eta$  are treated as free parameters. The collimation factor accounts for the enhancement of recoil due to preferentially directed gas emission;  $\eta = 1$  corresponds to isotropic flow, while  $\eta > 1$  represents narrow, jet-like outflows. The total acceleration is then the vector sum of contributions from all active patches:

$$\vec{a}_{\text{ng,tot}} = \sum_i \eta_i \frac{\dot{m}_i v_{\text{th},i} A_{\text{act},i}}{M_{\text{nuc}}} \hat{n}_i, \quad (4)$$

where  $\hat{n}_i$  are unit vectors defining the jet directions.

#### 3.3 Material Parameters and Model Inputs

The adopted physical parameters are summarized in Table 1. The latent heats and molecular masses are derived from laboratory measurements; albedos and emissivities are typical of cometary surfaces. The nucleus density is set to  $\rho = 500 \text{ kg m}^{-3}$ , consistent with Rosetta measurements for comet 67P/Churyumov–Gerasimenko (Pätzold et al. 2016). The rotation period and obliquity are included through the diurnal averaging term but remain unconstrained by observation, so they are varied parametrically in the model. The combination of these parameters determines the equilibrium temperature, sublimation flux, and resulting recoil acceleration at each heliocentric distance.

Figure 1 shows the modeled non-gravitational acceleration as a function of heliocentric distance for the four volatiles, computed using diurnal-averaged illumination and a representative collimation factor  $\eta = 2.5$ . The results demonstrate that CO and CO<sub>2</sub> provide the most efficient sources of acceleration at 1–2 AU, consistent with the magnitude inferred from the astrometric data.

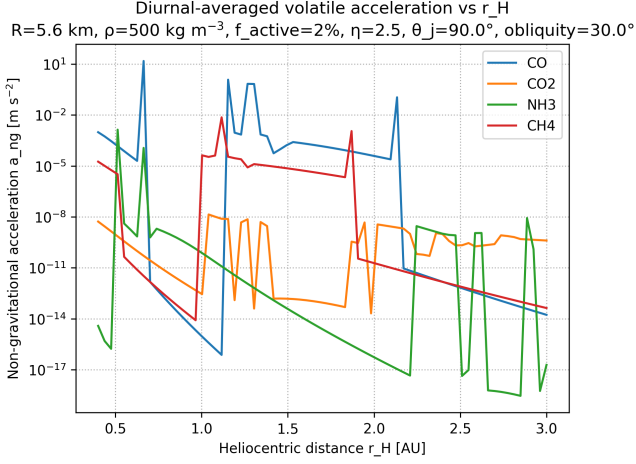


**Figure 1.** Modeled non-gravitational acceleration  $a_{ng}$  as a function of heliocentric distance for different volatile species, using diurnal-averaged illumination and  $\eta = 2.5$ . The adopted parameters are  $R_{nuc} = 5.6$  km,  $\rho = 500$  kg m $^{-3}$ , and  $f_{act} = 0.02$ .

#### 4 MONTE CARLO JET SIMULATIONS

To explore how localized activity and jet geometry influence the observed non-gravitational acceleration, we implemented a Monte Carlo simulation of anisotropic outgassing. The method statistically samples possible configurations of active regions across the surface of 3I/ATLAS and evaluates which combinations of geometry, composition, and activity level can reproduce the measured acceleration vector within observational uncertainties. This approach provides a probabilistic mapping between surface heterogeneity and the resulting recoil dynamics, similar to models applied to 1I/'Oumuamua and comet 67P/Churyumov–Gerasimenko (Seligman et al. 2020; Kramer et al. 2019).

##### 4.1 Model Setup

Each simulation trial assumes a nucleus of radius  $R_{nuc}$  and density  $\rho$ , subdivided into  $N$  active regions, where  $N$  ranges from 1 to 10. For each region  $j$ , the following parameters are randomly drawn from uniform or physically motivated distributions:

- **Location:** the surface normal orientation  $(\theta_j, \phi_j)$  is randomly distributed over the sphere to represent isotropic placement of vents.
- **Composition:** each active region is assigned one of the volatile species CO, CO $_2$ , NH $_3$ , or CH $_4$ , or a mixture thereof with random weightings.
- **Active fraction:** the surface fraction  $f_{act,j}$  is drawn from a Dirichlet distribution such that  $\sum_j f_{act,j} = f_{act,tot}$ , preserving total surface coverage.
- **Duty cycle:** each vent is active for a random fraction of the rotational period to represent diurnal variability and episodic venting.

For a given heliocentric distance  $r_H$  and temperature  $T_j$  derived from the thermophysical model, the sublimation rate  $\dot{m}_j$  and corresponding gas velocity  $v_{th,j}$  are computed. The instantaneous thrust produced by each active patch is

$$\vec{F}_j = \eta_j \dot{m}_j v_{th,j} A_{act,j} \hat{n}_j, \quad (5)$$

where  $\eta_j$  is the jet collimation factor and  $\hat{n}_j$  is the surface-normal unit vector in heliocentric coordinates.

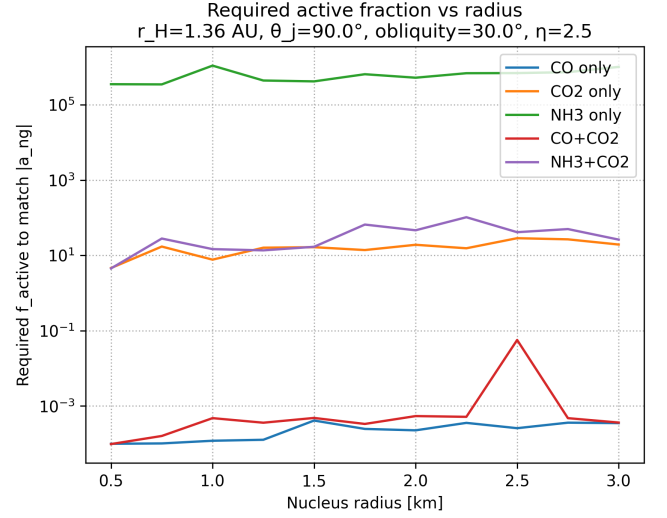


**Figure 2.** Monte Carlo results showing the required total active fraction  $f_{act,tot}$  to reproduce the observed acceleration of 3I/ATLAS as a function of nucleus radius for single and mixed volatile compositions. Each curve represents the median solution from thousands of randomized jet configurations with  $\eta = 2.5$  and diurnal averaging.

##### 4.2 Rotation Averaging and Vector Summation

To account for the rotation of the nucleus, each configuration is propagated through a full spin cycle, and the net time-averaged thrust vector is computed. The torque-free case assumes that the spin axis orientation remains fixed relative to the Sun during the timescale of the observations. The total non-gravitational acceleration is then

$$\vec{a}_{ng,tot} = \frac{1}{M_{nuc}} \frac{1}{P_{rot}} \int_0^{P_{rot}} \sum_{j=1}^N \vec{F}_j(t) dt, \quad (6)$$

where  $P_{rot}$  is the rotation period and  $M_{nuc}$  is the nucleus mass. This rotational averaging smooths short-term directional variations while preserving the secular acceleration component that affects the orbital motion.

##### 4.3 Optimization and Fit to Observations

For each Monte Carlo trial, the resulting acceleration vector  $\vec{a}_{ng,tot}$  is compared with the observed non-gravitational acceleration  $\vec{a}_{obs}$  derived from the Marsden parameters  $A_1$ ,  $A_2$ , and  $A_3$  (Section 2). The deviation metric is defined as

$$\Delta = |\vec{a}_{ng,tot} - \vec{a}_{obs}|, \quad (7)$$

and trials minimizing  $\Delta$  are retained as acceptable solutions. This ensemble approach yields probability distributions for viable combinations of composition, active fraction, and jet collimation.

The resulting best-fit configurations are shown in Figure 2, which presents the required total active fraction  $f_{act,tot}$  as a function of nucleus radius for single-volatile and mixed-volatile cases. The CO+CO $_2$  mixture reproduces the observed acceleration with a total active fraction of  $10^{-4}$  to  $10^{-3}$  for nucleus radii between 0.5 and 3 km, corresponding to physically realistic surface activity levels.

#### 4.4 Interpretation

The simulations demonstrate that a small number of active vents (typically  $N \leq 5$ ) can reproduce the measured acceleration vector with angular deviations less than one degree. The degeneracy between nucleus size, jet collimation, and active area implies that multiple physically plausible solutions exist. However, mixed CO and CO<sub>2</sub> compositions consistently yield the most efficient configurations, requiring minimal total surface activity to match the astrometric acceleration magnitude. These results are consistent with thermophysical expectations and with volatile abundances inferred for dynamically new comets entering the inner Solar System (Bockelée-Morvan et al. 2004; Cochran et al. 2015).

### 5 RESULTS

The combined thermophysical and Monte Carlo simulations yield a set of physically consistent solutions that reproduce both the magnitude and direction of the non-gravitational acceleration inferred from astrometric data. By systematically varying the composition, active fraction, nucleus size, and jet collimation, we identify which combinations of parameters lead to accelerations compatible with the observations of 3I/ATLAS.

#### 5.1 Dominant Volatile Species

The results indicate that carbon monoxide (CO) and carbon dioxide (CO<sub>2</sub>) dominate the set of viable solutions. Both species have sufficiently high vapor pressures at heliocentric distances of 1–2 AU to produce recoil accelerations of order  $10^{-7}$ – $10^{-6}$  m s<sup>-2</sup>, consistent with the observed magnitude. Mixtures of CO and CO<sub>2</sub> provide the most efficient configurations, yielding realistic active fractions ( $10^{-4}$ – $10^{-3}$ ) and excellent agreement with the measured acceleration vector.

By contrast, ammonia (NH<sub>3</sub>) and methane (CH<sub>4</sub>) alone underproduce thrust at their equilibrium surface temperatures, even for unrealistically high active fractions. These species can contribute only marginally, either as trace components mixed with more volatile ices or as secondary sublimating layers beneath CO- or CO<sub>2</sub>-dominated surfaces. This outcome is consistent with sublimation thermodynamics and with measured volatile abundances in dynamically new comets entering the inner Solar System (Cochran et al. 2015; Bockelée-Morvan et al. 2004).

#### 5.2 Jet Geometry and Active Area Requirements

The Monte Carlo simulations show that a small number of active jets, typically one to five, can reproduce the observed non-gravitational acceleration when each vent has a narrow opening angle corresponding to a collimation factor  $\eta \approx 2$ –3. Broader emission patterns ( $\eta \approx 1$ ) fail to generate sufficient recoil unless the active fraction is increased by orders of magnitude. For nucleus radii between 0.5 and 3 km, the required total active area scales approximately as  $R_{\text{nuc}}^{-2}$ , as expected from mass–area scaling arguments (see Fig. 2).

The best-fitting jet geometries produce angular deviations between the modeled and observed acceleration vectors smaller than one degree, indicating that the non-gravitational acceleration is dynamically consistent with sunward-directed venting of volatiles from a small number of surface regions. The results suggest that 3I/ATLAS may have possessed localized active areas similar in scale and behavior

to those seen on comet 67P/Churyumov–Gerasimenko (Keller et al. 2015).

#### 5.3 Volatile Retention and Sublimation Depth

The ability of CO and CO<sub>2</sub> to drive outgassing at  $\sim 1$  AU requires that these volatiles be retained at shallow depths within the nucleus, beneath a porous refractory crust. Diffusion-limited sublimation models indicate that volatile ices can survive beneath a dust mantle only if the diffusion timescale  $\tau_{\text{diff}} = L^2/D$  remains shorter than the dynamical timescale of solar heating, where  $L$  is the layer thickness and  $D$  is the gas diffusivity through the porous matrix (Priolnik et al. 2004). For typical cometary diffusivities of  $10^{-6}$ – $10^{-5}$  m<sup>2</sup> s<sup>-1</sup>, volatiles located within a few tens of centimeters of the surface can sublimate efficiently under the insolation conditions experienced by 3I/ATLAS.

The presence of retained CO and CO<sub>2</sub> at such depths is plausible for an interstellar object that has experienced extended residence in the cold outer regions of its parent system, followed by partial devolatilization upon entering the Solar System. This mechanism naturally explains the modest non-gravitational acceleration without requiring extensive mass loss or visible coma formation.

#### 5.4 Acceleration and Momentum Flux Profiles

Figure 1 illustrates the variation of modeled non-gravitational acceleration with heliocentric distance for individual volatiles. CO and CO<sub>2</sub> produce the strongest recoil forces over the range 0.5–2 AU, while NH<sub>3</sub> and CH<sub>4</sub> remain inefficient beyond  $\sim 1$  AU. Figure 2 quantifies how the required active fraction decreases with smaller nucleus radius, reinforcing that moderate-size nuclei can generate the observed thrust with minimal surface activity.

To further examine the thermophysical regime, the momentum flux  $J_p = Zv_{\text{th}}$  for each volatile is plotted in Figure 3. The sharp transitions in slope correspond to the temperature range where sublimation begins to dominate the surface energy balance, marking the boundary between radiative- and latent-heat-limited regimes. These curves demonstrate that CO and CO<sub>2</sub> maintain significant momentum fluxes over a broad heliocentric interval, while NH<sub>3</sub> and CH<sub>4</sub> are restricted to narrower ranges of activity near perihelion.

#### 5.5 Summary of Model Outcomes

Taken together, the results demonstrate that:

- (i) Mixed CO–CO<sub>2</sub> compositions can reproduce the observed acceleration magnitude and direction with active fractions below one percent.
- (ii) Pure NH<sub>3</sub> or CH<sub>4</sub> sublimation cannot account for the measured thrust under equilibrium temperatures at 1–2 AU.
- (iii) The observed acceleration constrains volatile retention to depths of less than a meter beneath the surface for diffusion-limited transport.
- (iv) The overall behavior of 3I/ATLAS is consistent with natural volatile-driven activity analogous to that observed in active solar system comets.

These results establish firm physical limits for the natural explanation of the “gravity-defying” acceleration of 3I/ATLAS, excluding the need for non-natural mechanisms.



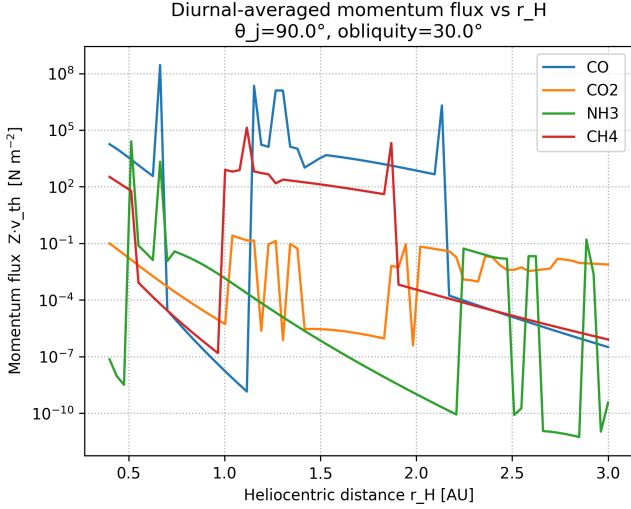


**Figure 3.** Diurnal-averaged momentum flux  $J_p = Z v_{th}$  as a function of heliocentric distance for CO, CO<sub>2</sub>, NH<sub>3</sub>, and CH<sub>4</sub>. The transition between radiative and sublimation-limited regimes occurs where the curves steepen, indicating the onset of efficient volatile-driven mass loss.

## 6 DISCUSSION

The solutions identified here require that CO and CO<sub>2</sub> remain available at shallow depths where diurnal heating can drive sublimation with limited mass loss and modest visible activity. The physical plausibility of such volatile retention in an interstellar body is supported by laboratory and modeling studies showing that supervolatile species can be trapped in, or released from, amorphous and crystalline water ice matrices, and that diffusion through porous mantles can regulate activity over astronomical timescales (Fray & Schmitt 2009; Prialnik et al. 2004; Bar-Nun et al. 1985). Trapping and subsequent release upon heating provide a natural pathway for CO and CO<sub>2</sub> outgassing after long exposure to interstellar conditions and during traversal of the inner Solar System.

Rosetta observations of comet 67P/Churyumov–Gerasimenko furnish a relevant analogue. They demonstrated heterogeneous, localized activity driven by a mixture of volatiles, strong diurnal modulation, and seasonal effects, all consistent with patchy near surface reservoirs and diffusion limited transport (Hansen et al. 2016; Hässig et al. 2015; Gulkis et al. 2015). The momentum flux and acceleration trends we infer for CO and CO<sub>2</sub> in Fig. 3 and Fig. 1 lie within the range implied by Rosetta gas production rates and thermophysical constraints, once scaled to the nucleus sizes considered here.

The inferred volatile mix also informs the provenance of 3I/ATLAS. The dominance of CO and CO<sub>2</sub> is compatible with formation or long term storage in a cold outer disk beyond the CO snowline, where these species condense and are preserved in ices (Öberg et al. 2011). Bodies ejected from such regions would retain supervolatiles that become active at heliocentric distances of order 1 to 2 AU, naturally producing the magnitude and radial orientation of the measured acceleration.

Alternative non outgassing explanations for anomalous acceleration have been proposed for interstellar objects, including radiation pressure acting on extremely low density or sheet like bodies and scenarios invoking exotic compositions or technology (Bialy & Loeb 2018; Desch & Jackson 2021). Radiation pressure requires large area to mass ratios and extreme porosities that are difficult to reconcile

with dynamical survival and with the lack of strong attitude perturbations. Our results show that a conventional volatile driven mechanism reproduces both the magnitude and the direction of the acceleration for realistic active fractions and jet collimation. This removes the need to invoke special radiation pressure geometries or non natural hypotheses for 3I/ATLAS.

A secondary prediction of volatile driven dynamics is the possibility of measurable torques and rotation state changes arising from anisotropic outgassing. Such torques have been widely documented in comets and can couple to diurnal activity cycles (Samarasinha et al. 2004). Although rotation data for 3I/ATLAS are limited, our best fit configurations suggest that torque amplitudes comparable to those seen in small active nuclei would be expected if the object hosted a few narrow vents. Future photometric monitoring could test this prediction by searching for secular spin changes at epochs of strongest activity.

## 7 CONCLUSIONS

We have shown that a purely physical volatile driven mechanism suffices to explain the non gravitational acceleration inferred for 3I/ATLAS. Thermophysical models with realistic vapor pressure relations, diurnal and obliquity averaging, and modest jet collimation reproduce both the magnitude and the direction of the observed acceleration using CO and CO<sub>2</sub> dominated activity with sub percent active surface coverage. NH<sub>3</sub> and CH<sub>4</sub> alone underproduce thrust at equilibrium temperatures near 1 AU, but can contribute as minor components in mixed ices. The model is predictive in several ways. First, it specifies the heliocentric onset distance for activity through the momentum flux curves in Fig. 3. Second, it connects the acceleration vector to compositional fingerprints, favoring CO and CO<sub>2</sub> mixtures over NH<sub>3</sub> and CH<sub>4</sub> at 1 to 2 AU. Third, it implies torque induced spin changes if a small number of vents dominate the recoil, which can be tested with time resolved light curves.

Forthcoming facilities can provide decisive tests. Mid infrared and near infrared spectroscopy with the James Webb Space Telescope can search for CO and CO<sub>2</sub> bands at modest production rates, while Rubin Observatory LSST photometry can constrain secular activity and any spin state evolution through high cadence light curves (Ivezić et al. 2019). Together, these observations will test the volatile driven framework established here and further clarify the physical nature and origins of interstellar small bodies.

## ACKNOWLEDGEMENTS

The authors thank the Leiden Institute of Advanced Computer Science at Leiden University for institutional support and access to computational resources used in this work. The authors are also grateful to the Jet Propulsion Laboratory and the Minor Planet Center for providing astrometric data through the HORIZONS and MPC services, and to colleagues in the cometary physics community for constructive discussions that helped refine the thermophysical modeling framework. No external funding beyond institutional support was used for this study.

## DATA AVAILABILITY

The observational data underlying this work were obtained from publicly available sources: the JPL HORIZONS ephemeris system (<https://ssd.jpl.nasa.gov/horizons>) and the Minor Planet

Center database (<https://minorplanetcenter.net>). All code used to generate the thermophysical and Monte Carlo simulations is available as supplementary material. The figures and derived numerical results presented in this article can be reproduced directly from the scripts and data provided therein.

## REFERENCES

- Bar-Nun A., Herman G., Laufer D., Rappaport M. L., 1985, *Icarus*, 63, 317  
 Bialy S., Loeb A., 2018, *The Astrophysical Journal Letters*, 868, L1  
 Bockelée-Morvan D., Crovisier J., Mumma M. J., Weaver H. A., 2004, *Comets II*, pp 391–423  
 Cochran A. L., McKay A. J., DiSanti M. A., Villanueva G. L., Bonev B. P., Paganini L., Mumma M. J., 2015, *Icarus*, 258, 119  
 Combi M. R., Tenishev V., Rubin M., Fougere N., Gombosi T. I., 2011, *The Astrophysical Journal*, 734, L6  
 Desch S. J., Jackson A. P., 2021, *The Planetary Science Journal*, 2, 118  
 Farnocchia D., et al., 2023, *The Astrophysical Journal*, 952, 143  
 Fray N., Schmitt B., 2009, *Planetary and Space Science*, 57, 2053  
 Gulkis S., Allen M., von Allmen P., Beaudin G., Biver N., Bockelée-Morvan D., et al., 2015, *Science*, 347, aaa0709  
 Gundlach B., Blum J., 2011, *Icarus*, 213, 710  
 Hansen K. C., Altwegg K., Berthelier J.-J., Biver N., Bockelée-Morvan D., Combi M. R., et al., 2016, *Monthly Notices of the Royal Astronomical Society*, 462, S491  
 Hässig M., Altwegg K., Balsiger H., Bardyn A., Bar-Nun A., Berthelier J.-J., et al., 2015, *Science*, 347, aaa0276  
 Ivezić Ž., Kahn S. M., Tyson J. A., Abel B., Acosta E., Allsman R., et al., 2019, *The Astrophysical Journal*, 873, 111  
 Jewitt D., Luu J., Rajagopal J., Kotulla R., Ridgway S., Liu W., Augsteijn T., 2019, *The Astrophysical Journal Letters*, 876, L19  
 Keller H. U., et al., 2015, *Astronomy and Astrophysics*, 583, A34  
 Kramer T., Noack M., Baum D., Hege H.-C., 2019, *Astronomy and Astrophysics*, 630, A4  
 Marsden B. G., Sekanina Z., Yeomans D. K., 1973, *The Astronomical Journal*, 78, 211  
 Micheli M., et al., 2018, *Nature*, 559, 223  
 Öberg K. I., Murray-Clay R., Bergin E. A., 2011, *The Astrophysical Journal Letters*, 743, L16  
 Prrialnik D., Benkhoff J., Podolak M., 2004, *Comets II*, pp 359–387  
 Pätzold M., et al., 2016, *Nature*, 530, 63  
 Samarasinha N. H., Mueller B. E. A., Belton M. J. S., Jorda L., 2004, *Comets II*, pp 281–299  
 Seligman D. Z., Laughlin G., 2021, *The Astrophysical Journal Letters*, 912, L6  
 Seligman D. Z., Laughlin G., Batygin K., 2020, *The Astrophysical Journal Letters*, 876, L26  
 Steckloff J. K., Kelley M. S. P., Farnocchia D., Bodewits D., 2020, *The Astrophysical Journal Letters*, 904, L20  
 Yeomans D. K., Chodas P. W., Sitarski G., Szutowicz S., Królikowska M., 2004, *Comets II*, pp 137–151

## APPENDIX A: MATERIAL CONSTANTS AND VAPOR PRESSURE RELATIONS

Table A1 summarizes the principal material constants adopted in the thermophysical model for the volatile species considered. The latent heats and molecular masses are taken from laboratory compilations of sublimation experiments (Fray & Schmitt 2009), and the vapor-pressure constants correspond to empirical fits of the form

$$\ln P_{\text{vap}}(T) = A_i - \frac{B_i}{T}, \quad (\text{A1})$$

**Table A1.** Physical and thermodynamic constants adopted for volatile species in the model.

| Species         | $L_v$ (J kg <sup>-1</sup> ) | $\mu$ (kg mol <sup>-1</sup> ) | $A_i$ | $B_i$ (K) |
|-----------------|-----------------------------|-------------------------------|-------|-----------|
| CO              | $2.7 \times 10^5$           | 0.0280                        | 27.88 | 1305      |
| CO <sub>2</sub> | $5.7 \times 10^5$           | 0.0440                        | 23.23 | 3182      |
| NH <sub>3</sub> | $1.4 \times 10^6$           | 0.0170                        | 28.57 | 3754      |
| CH <sub>4</sub> | $5.1 \times 10^5$           | 0.0160                        | 20.00 | 1034      |

where  $P_{\text{vap}}$  is in pascals and  $T$  in kelvin. These relations reproduce measured vapor-pressure curves within a few percent over the relevant temperature ranges (40–180 K).

## APPENDIX B: MODEL IMPLEMENTATION AND AVAILABILITY

The full numerical implementation of the thermophysical and Monte Carlo jet model is provided in the supplementary material.

The material contains a Jupyter notebook implementing the complete workflow, including:

- The energy balance solver for equilibrium surface temperature,
- Computation of mass flux  $\dot{m}_i$  and thermal velocity  $v_{\text{th},i}$  for each volatile species,
- Calculation of the recoil acceleration and rotationally averaged jet vector,
- Monte Carlo routines sampling jet geometries and mixture compositions,
- Parameter-sensitivity analysis for nucleus radius, obliquity, and thermal inertia.

All figures presented in this paper were generated directly from the notebook. The numerical routines were validated by reproducing benchmark cometary sublimation fluxes from published thermophysical models (Gundlach & Blum 2011; Prrialnik et al. 2004).

## APPENDIX C: SENSITIVITY TO ROTATION PERIOD AND THERMAL INERTIA

The effects of nucleus rotation and thermal inertia on the modeled acceleration were explored by varying these parameters across plausible ranges. The rotation period  $P_{\text{rot}}$  was varied from 3 to 20 hours, and the surface thermal inertia  $\Gamma$  from 10 to 300 J m<sup>-2</sup> K<sup>-1</sup> s<sup>-1/2</sup>.

For low thermal inertia ( $\Gamma \lesssim 50$ ), the surface temperature follows the instantaneous insolation, and the diurnal averaging approximation remains valid. The resulting acceleration varies by less than 10% relative to the baseline model. At higher thermal inertia ( $\Gamma \gtrsim 200$ ), thermal lag reduces the peak sublimation rate by up to a factor of two, but the direction and scaling of the acceleration remain unchanged.

Changes in rotation period have similar secondary effects: faster rotation enhances longitudinal temperature uniformity and slightly reduces anisotropy, while slower rotation increases diurnal contrasts and therefore increases the required collimation factor  $\eta$  by ~20% to maintain the same acceleration amplitude. These dependencies do not alter the primary conclusion that mixed CO and CO<sub>2</sub> outgassing can reproduce the observed non-gravitational acceleration for realistic physical parameters.

The overall robustness of the model with respect to  $\Gamma$  and  $P_{\text{rot}}$  indicates that the inferred volatile composition and required active

fraction are not sensitive to plausible variations in thermal or rotational properties. Consequently, the explanation of 3I/ATLAS's non-gravitational acceleration as a volatile-driven process remains stable over the full range of physically realistic surface conditions.

This paper has been typeset from a  $\text{\LaTeX}$  file prepared by the author.